JOURNAL OF MATERIALS SCIENCE 32 (1997) 1325–1332

Preparation and properties of stable dysprosium-doped α-sialon ceramics

ZHIJIAN SHEN
Department of Materials Science and Engineering, Zhejiang University, Hangzhou 310027, People's Republic of China

T. EKSTRÖM, M. NYGREN
Department of Inorganic Chemistry, Arrhenius Laboratory, University of Stockholm, S-106 92 Stockholm, Sweden

Dense ceramics with overall compositions $Dy_xSi_{12-4.5x}Al_{4.5x}O_{1.5x}N_{16-1.5x}$, where $0.2 \leqslant x \leqslant 1.0$, along the Si_3N_4–$Dy_2O_3 \cdot 9AlN$ tie line were prepared by hot-pressing at 1800 °C. The dysprosium-doped α-sialon phase formed in the composition range $0.3 \leqslant x \leqslant 0.7$. Sintered materials of different compositions were post-heat-treated at temperatures in the range 1300–1750 °C for different times and it was shown that the Dy-α-sialon phase is stable over a large temperature interval and during heat treatment times up to 30 days. Unlike corresponding neodymium- and samarium-doped α-sialons, dysprosium-doped α-sialon does not decompose into β-sialon and rare-earth-rich grain-boundary phase(s) at temperatures below 1550 °C. The α-phase can coexist with a liquid phase at temperatures $\geqslant$ 1550 °C and with the Dy-M′-phase ($Dy_2Si_{3-x}Al_xO_{3+x}N_{4-x}$) at lower temperatures. When heat treated at 1450 °C, any residual liquid grain-boundary phase reacted with minor amounts of the α-sialon phase and devitrified to Dy-M′-phase, yielding a glassy phase-free material. The Dy-M′-phase formed had the maximum aluminium substitution, i.e. $x \approx 0.7$. Dysprosium-doped α-sialon exhibited very high hardness ($H_{v_{10}} = 22$ GPa) and a fracture toughness of 4.5 $MPam^{1/2}$, and the hardness and toughness decreased only slightly after devitrification of the glassy phase. Some elongated α-sialon grains were formed at high x values in glassy phase-containing materials, but their presence did not affect the toughness significantly.

1. Introduction

Among the materials formed in the Me–Si–Al–O–N systems, the pure α-sialon ceramics show excellent thermal shock resistance and the ultimate hardness achievable for these silicon nitride-based materials, with a Vickers hardness ($H_{v_{10}}$) around 21 GPa. The presence of α-sialon contributes to the hardness in the important α–β sialon composites, which in turn gives a favourable property combination for many applications [1–5]. It is also evident from its chemical composition that α-sialon offers the possibility of reducing the amount of residual glassy grain-boundary phase by incorporating constituents of the sintering aids into the crystal structure, which otherwise will be present as substantial amounts of residual glassy phase and deteriorate the high-temperature performance of the materials. Thus α-sialon enables the preparation of glass-free sialon composites, which may become interesting candidates for high-temperature structural applications.

The α-sialon solid solution has a fairly limited two-dimensional extension in the plane Si_3N_4–$Al_2O_3 \cdot AlN$–$MeN \cdot 3AlN$ of the Jänecke's prism commonly used illustrating phase relations in Me–Si–Al–O–N system [6–8]. α-sialon, isostructural with α-Si_3N_4, has an overall composition given by the formula of $Me_xSi_{12-(m+n)}Al_{m+n}O_nN_{16-n}$, where m(Si–N) bonds are replaced by m(Al–N) bonds and n(Si–N) bonds are replaced by n(Al–O) bonds. The charge discrepancy introduced by the former substitution mechanism is compensated by the metal ion Me^{p+}, with $m = px$. There are two interstitial sites per unit cell in the α-Si_3N_4 structure that can be occupied by these Me^{p+} metal ions, and this yields the limit $x \leqslant 2$ in the formula above, because each unit cell contains four formula units. α-Si_3N_4 is regarded as a low-temperature modification of Si_3N_4, but the α-sialon modification is stable at higher temperatures due to incorporation of Me^{p+} metal ions in its network [6]. The Me-elements which have been reported to stabilize the α-sialon modification are lithium, magnesium, calcium, yttrium, and the rare-earth metals, except cerium, lanthanum, praseodymium and europium. For yttrium and for the rare-earth metals, the minimum amount of occupancy is around 7.5% and the maximum around 50% [7, 8].

0022–2461 © *1997 Chapman & Hall*

Although the α-sialon structure can be stabilized by many different Me^{p+} cations, the most precisely described α-sialon is that stabilized by yttrium. In this case, the solid solubility limits have been thoroughly investigated, and several studies have described the reaction sequences and the mechanical properties [2, 3]. Thus, there are previous studies which show that the transformation between α- and β-silicon nitride, which takes place at temperatures exceeding 1350 °C, is a reconstructive polymorphic transformation, while the transformation between α- and β-sialon is essentially chemically controlled [6]. Accordingly, the phase assembly obtained in the final product is thought to be determined by the overall composition of the starting material, while processing parameters such as temperature, pressure and heating and cooling rates are believed to be of less importance [3].

However, it was surprisingly shown recently by Mandal *et al.* [9] and by Ekström and Shen [10] that the cooling rate applied after sintering determines the microstructure of α-sialon containing ceramics to a great extent. Some rare-earth stabilized α-sialons thus seemed to be unstable at temperatures below 1600 °C and transformed to β-sialon and other phases. Because α- and β-sialon offer different mechanical properties, these findings may open a new possibility of tailoring the microstructures and properties of sialon-based materials [9].

Our present work, therefore, was devoted to studies of the thermal and time stability of different rare-earth-doped α-sialon phases both in pure α- and mixed α–β sialon systems. In this connection we have shown that for certain rare-earth dopants, the α-sialon modification is stable only at high temperatures and can, totally or partly, be transformed into the β-sialon modification and rare-earth-rich grain-boundary phase(s) by subsequent heat treatment in the temperature range 1000–1450 °C [10–13]. The degree and/or speed of transformation were found to be fairly complex and depend primarily on the rare-earth element used, but also on the starting composition, the amount/composition of the liquid involved in the system at the sintering temperature and the type/amount of grain-boundary phase(s) formed after heat treatment. This reaction was found to be reversible, i.e. the original α-sialon phase was reformed by subsequent heat treatment above or at 1550 °C [9, 11–13].

In this paper we will describe the formation, thermal and time stability of the α-sialon in dysprosium-doped α-sialon ceramics with overall compositions along the Si_3N_4–$Dy_2O_3 \cdot 9AlN$ join line. These materials have been post-heat-treated in different ways and quenched to room temperature after the heat treatment in order to reveal the phase composition at elevated temperatures. The results are discussed and compared with previous findings reported by us and other workers. The mechanical properties ($H_{v_{10}}$ and K_{1c}) of samples heat treated in various ways are also discussed.

2. Experimental procedure

All samples prepared in the present work were designed to cover the α-sialon solid-solution range along the Si_3N_4–$Dy_2O_3 \cdot 9AlN$ join line. Thus, overall compositions of $Dy_xSi_{12-4.5x}Al_{4.5x}O_{1.5x}N_{16-1.5x}$ with $x = 0.2, 0.25, 0.35, 0.4, 0.6, 0.7, 0.8$ and 1.0, were prepared. The starting powders were Si_3N_4 (UBE, SN-E10), AlN (H.C. Starck-Berlin, grade A), and Dy_2O_3 (99.9%, Johnson Matthey Chemicals Ltd). The dysprosium oxide powder was calcined at 1000 °C for 2 h before use. In the preparation of the samples, corrections were made for the small amounts of oxygen present in the Si_3N_4 and AlN raw materials. The analysed oxygen content of silicon nitride powder corresponded to 2.74 wt % SiO_2 and of the aluminium nitride powder to 1.9 wt % Al_2O_3. The overall compositions of the starting materials are given in Table I.

The starting material mixes were milled in water-free propanol for 24 h in a plastic jar, using sialon milling media, and the batch size used was 50 g. Pellets of dried powders (about 5 g) were first compacted in a steel die, followed by hot pressing in BN-coated graphite dies at 1800 °C (25–32 MPa pressure, holding time 2 h) in a graphite resistance furnace under a protective nitrogen atmosphere, and were allowed to cool in the furnace (cooling rate 50 °C min^{-1}).

Selected specimens were subsequently heat treated in different ways. Some samples were placed in a carbon crucible embedded in a powder mixture of Si_3N_4, AlN and BN and re-heated up to 1750 °C in a graphite furnace in nitrogen atmosphere. After 30 min holding time, the samples were either quenched to room temperature (at a rate of approximately 400 °C min^{-1} in the critical temperature range 1650–1000 °C) by quickly moving them to a cooling chamber attached to the graphite furnace, or rapidly cooled to 1650 or 1550 °C. At the latter temperatures the samples were held for another 24 h and then quenched. Some of the hot-pressed samples (embedded in the powder mixture described above) were re-heated up to 1450 or 1300 °C in a nitrogen atmosphere and were held at this temperature for extended times (up to 30 days).

The densities of the sintered specimens were measured according to Archimedes' principle. Before physical characterization, the specimens were carefully polished by standard diamond-polishing techniques. Hardness, $H_{v_{10}}$, and indentation fracture toughness, K_{1c}, at room temperature were obtained using a Vickers diamond indentor with a 98 N (10 kg) load, and the fracture toughness was evaluated according to the method of Anstis *et al.* [14], assuming a value of 300 GPa for Young's modulus.

TABLE I Overall compositions of the starting materials

Sample	x	Dy_2O_3 (wt%)	Si_3N_4 (wt%)	AlN (wt%)
ADY02	0.2	6.36	87.14	6.50
ADY025	0.25	7.72	84.62	7.66
ADY035	0.35	10.25	79.03	10.72
ADY04	0.4	11.60	76.30	12.10
ADY06	0.6	16.67	66.28	17.05
ADY07	0.7	19.29	61.53	19.18
ADY08	0.8	21.27	57.16	21.57
ADY10	1.0	25.72	48.70	25.58

Analyses of the crystalline phases of the prepared samples were based on their X-ray powder diffraction (XRD) records obtained in a Guinier–Hägg focusing camera with CuK_{α_1} radiation and silicon as internal standard. The photographs were evaluated with a computer-linked SCANPI system [15], and the cell parameters were determined with use of the program PIRUM [16]. The z-value of the β-sialon phase $Si_{6-z}Al_zO_zN_{8-z}$ was obtained according to the unit cell dimensions, using the equations given elsewhere [17].

In the semi-quantitative estimation of the amounts of crystalline phases, the integrated intensities of the following reflections were used: (i) (1 0 2) and (2 1 0) of the α-sialon; (ii) (1 0 1) and (2 1 0) of the β-sialon; (iii) (1 0 1) and (0 1 2) of the 21-R polytype; (iv) (2 1 1) of the dysprosium-melilite phase. The relative fraction of each phase was then calculated from the expression

$$W_k = (I_k) \Big/ \sum_{i=1}^{n} (I_i) \quad 1 \leqslant k \leqslant n \tag{1}$$

where W_k is the fraction of phase k, and n is the number of crystalline phases present.

After application of a carbon coating to the polished surfaces of hot-pressed and heat-treated samples, these surfaces were examined in a scanning electron microscope (Jeol JSM 820, equipped with a Link AN 10 000 EDS analyser). For some of the samples, the silicon, aluminium and dysprosium contents of the α-sialon grains were determined by EDS analysis, using calibration curves. The final results reported below are averages of at least five experimental point determinations.

3. Results and discussion

All the hot-pressed samples were found to be fully densified, and the density increased linearly with increasing amount of the heavy element dysprosium, as expected. The measured densities as a function of overall x values for samples hot-pressed and heat-treated in different ways are summarized in Fig. 1. The densification was also confirmed by optical microscopy and microstructural SEM studies of polished cross-sections, as no porosity was observed. The samples re-heated to 1750 °C and held for longer periods at different high temperatures had suffered weight losses of about 1–2 wt %, despite the use of a powder bed, which may be attributed to a loss mainly of SiO. This is, however, not likely to change the observed results significantly.

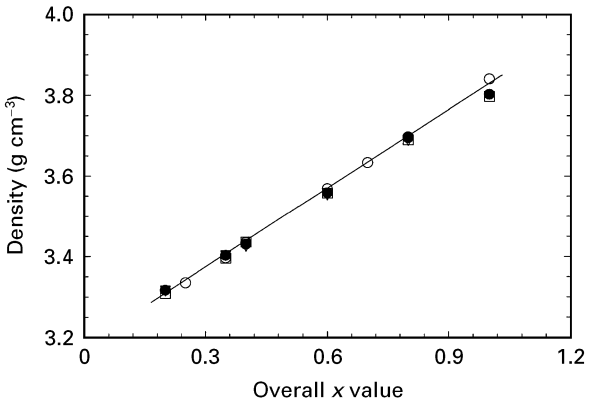

Figure 1 Density as a function of the overall composition represented by x value for samples along the Si_3N_4–$Dy_2O_3 \cdot 9AlN$ tie line. (○) Hot-pressed materials, (□) hot-pressed samples re-heated and quenched from 1750 °C, (●) hot-pressed samples re-heated at 1450 °C for 24 h, (▽) samples heat treated at 1300 °C for 24 h.

3.1. Homogeneity region of the α-sialon phase along the Si_3N_4–$Dy_2O_3 \cdot 9AlN$ tie line

The phase contents determined by XRD of hot-pressed and furnace-cooled samples ($T_{cool} \approx 50$ °C min^{-1}) as a function of their overall compositions (x value) are illustrated in Fig. 2a. The obtained materials can be divided mainly into three areas, I–III. In the first area (I), with overall x values in the range $0 < x < 0.35$, the main crystalline phases are α- and β-sialon. In the second area (II), with overall x values in the range $0.35 \leqslant x < 0.6$, α-sialon is the principal crystalline component. In the third area (III), with x values larger than 0.6, the main crystalline phase component is still α-sialon but aluminium-containing dysprosium-melilite phase ($Dy_2Si_{3-x}Al_xO_{3+x}N_{4-x}$, denoted M′-phase below) is always present in increasing amounts with increasing x value. The 21R sialon polytypoid is also formed in the latter compositional area.

The hot-pressed materials were re-heated up to 1750 °C, held at this temperature for 30 min to equilibrate, and then quenched to room temperature. The results of the phase analysis are compiled in Fig. 2b. The phase assembly in the hot-pressed and quenched samples was very similar, the main difference being that the Dy-M′-phase present in the hot-pressed samples with x values between 0.6 and 0.7 and below 0.35 was dissolved by the re-heating. These results indicate that M′-phase is formed very rapidly during the cooling process, and the formation can only be inhibited by quenching.

The hot-pressed samples were also heat treated at 1450 °C for 24 h. In this case, more M′-phase was obtained in all samples, accompanied by a decrease of the α-sialon content as illustrated in Fig. 2c.

The observed hexagonal unit cell dimensions of α-sialons in the hot-pressed samples, those quenched from 1750 °C and those heat treated at 1450 °C are given in Fig. 3 as functions of the overall x values. The α-sialon unit cell expands noticeably in both the a and c directions with increase of the overall x value, and there is a tendency for the unit-cell dimensions to decrease by post-heat-treatment for samples with x values larger than 0.6. This implies that some kind of reaction between α-sialon and residual grain-boundary liquid phase may take place during the post-heat-treatment process, crystallizing M′-phase and leading to a slight composition shift of α-sialon in these samples.

Microstructure studies (discussed in more detail below) revealed that a residual dysprosium-rich

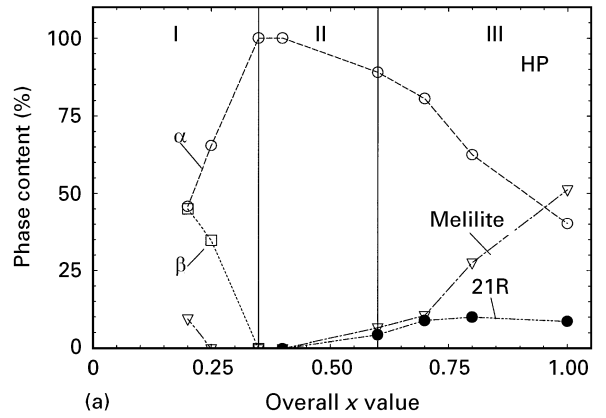

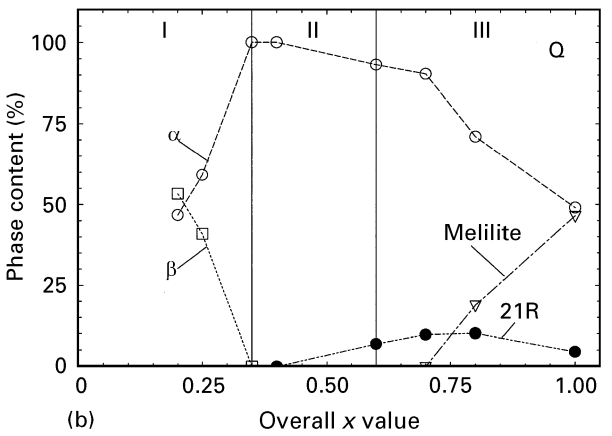

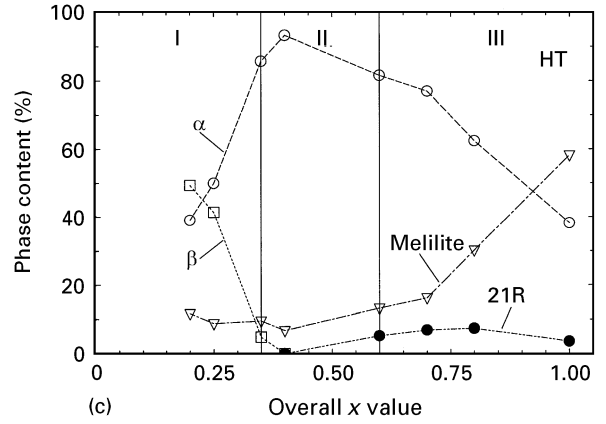

Figure 2 Phase content as a function of overall composition, x, for (a) hot-pressed samples, (b) samples quenched from 1750 °C, and (c) samples heat treated at 1450 °C for 24 h and then quenched.

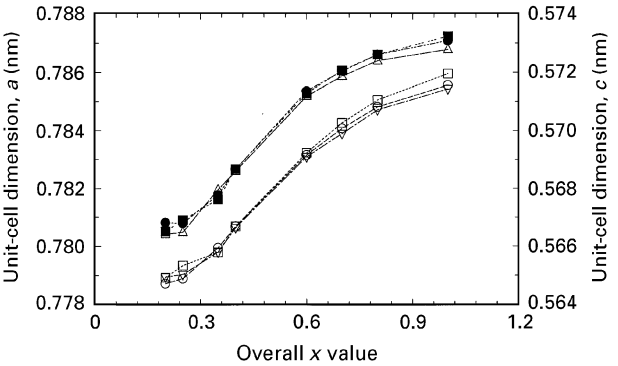

Figure 3 Unit-cell dimensions of the α-sialon phase as function of the overall composition, x, of materials prepared by (○) hot-pressing, (□) quenching from 1750 °C, and (▽) after being heat treated at 1450 °C for 24 h. (□, ○, ▽) a, (■, ●, ▼) c.

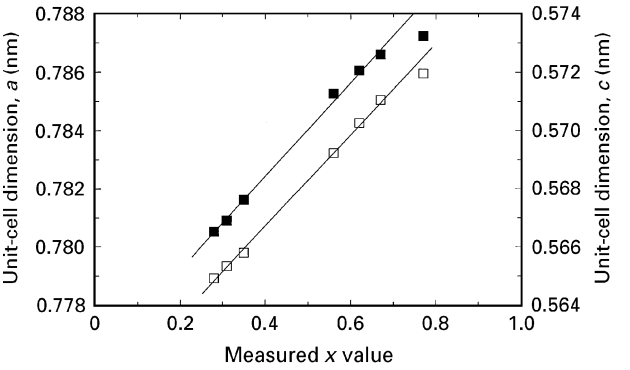

Figure 4 Unit-cell dimensions of the formed α-sialon as function of the measured composition, x, of individual grains, as determined by EDS for samples quenched from 1750 °C, cf. text. (□) a, (■) c.

intergranular phase was present in all samples, and the amount of this phase increased with increasing overall x value. As the intergranular phase contained appreciable amounts of the rare-earth element, the dysprosium-content of the α-sialon must be different from that given by the overall composition. This prompted us to determine the actual metal content of the α-sialon grains in samples quenched from 1750 °C by EDS point analysis. The lattice parameters of the α-sialon phase are thus plotted against these measured x values in Fig. 4, and the increase of α-sialon unit cell dimensions with measured x values can be expressed as

$$a = 0.775 + 0.0156x \text{ nm} \quad (2a)$$

$$c = 0.562 + 0.0162x \text{ nm} \quad (2b)$$

The obtained results show that α-sialon forms in the composition region with x values from 0.3 to about 0.7, which is wider than that in neodymium and samarium systems ($0.3 \leqslant x \leqslant 0.5$ and $0.3 \leqslant x \leqslant 0.6$, respectively) but narrower than that in ytterbium system, where $0.3 \leqslant x < 1.0$ [11–13]. The observed extended solid solution area agrees with previous studies on subsolidus phase relationships in Si_3N_4–AlN–rare-earth oxide systems, showing that the solid solubility limit of α-sialon in these systems widens with decreasing ionic radii of the rare-earth cations [7].

According to the formula $Dy_xSi_{12-4.5x}Al_{4.5x}O_{1.5x}N_{16-1.5x}$, the Si/Al atomic ratio of pure α-sialon on the Si_3N_4–$Dy_2O_3 \cdot 9AlN$ line can be expressed as

$$\text{Si/Al} = 2.667x^{-1} - 1 \quad (3)$$

and this function is drawn as a solid line in Fig. 5. Measured Si/Al atomic ratios of the α-sialon phase in the samples quenched from 1750 °C are also plotted versus the measured x value. It is evident that the calculated and observed Si/Al ratios in the single-phase α-sialon range $0.3 \leqslant x \leqslant 0.7$, are in good agreement with each other.

The sample with the lowest x value has a somewhat higher observed Si/Al ratio, and one reason might be that as this material is positioned in a multi-phase area, the α-sialon in equilibrium with β-sialon has changed its composition somewhat from that set by

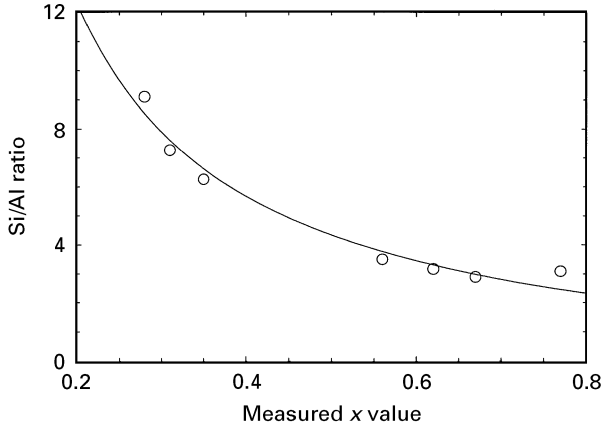

Figure 5 Si/Al atomic ratio in α-sialon according to the formula $Dy_xSi_{12-4.5x}Al_{4.5x}O_{1.5x}N_{16-1.5x}$ plotted versus by the EDS-measured x value of samples quenched from 1750 °C.

the overall composition towards a composition close to the boundary of the three-phase α/β/liquid region, i.e. the α-sialon will have higher Si/Al and N/O ratios [8].

The sample with the highest x value also showed a higher Si/Al ratio than the calculated one and a smaller increase of the unit cell dimensions, which in this case might be due to the fact that the formed α-sialon also shifted the composition to more silicon- and oxygen-rich compositions. This sample is in a multi-phase region; and formation of the 21R sialon polytypoid will "consume" Al–N units, and the formed Dy–M′- phase will "consume" Al–O. The Dy-M′-phase in this sample has $x = 0.7$ according to the EDS point analysis and also according to the lattice parameters, using the composition-lattice parameter relation given elsewhere [18].

Scanning electron micrographs (obtained in back-scattered electron mode) of typical samples quenched from 1750 °C are given in Fig. 6. The α-sialon appears with grey contrast in the micrographs, and the dysprosium-rich crystalline and amorphous intergranular phases are white. The occurrence of elongated β-sialon crystals in some samples (with low overall x values) is easily detected by their elongated shape and black

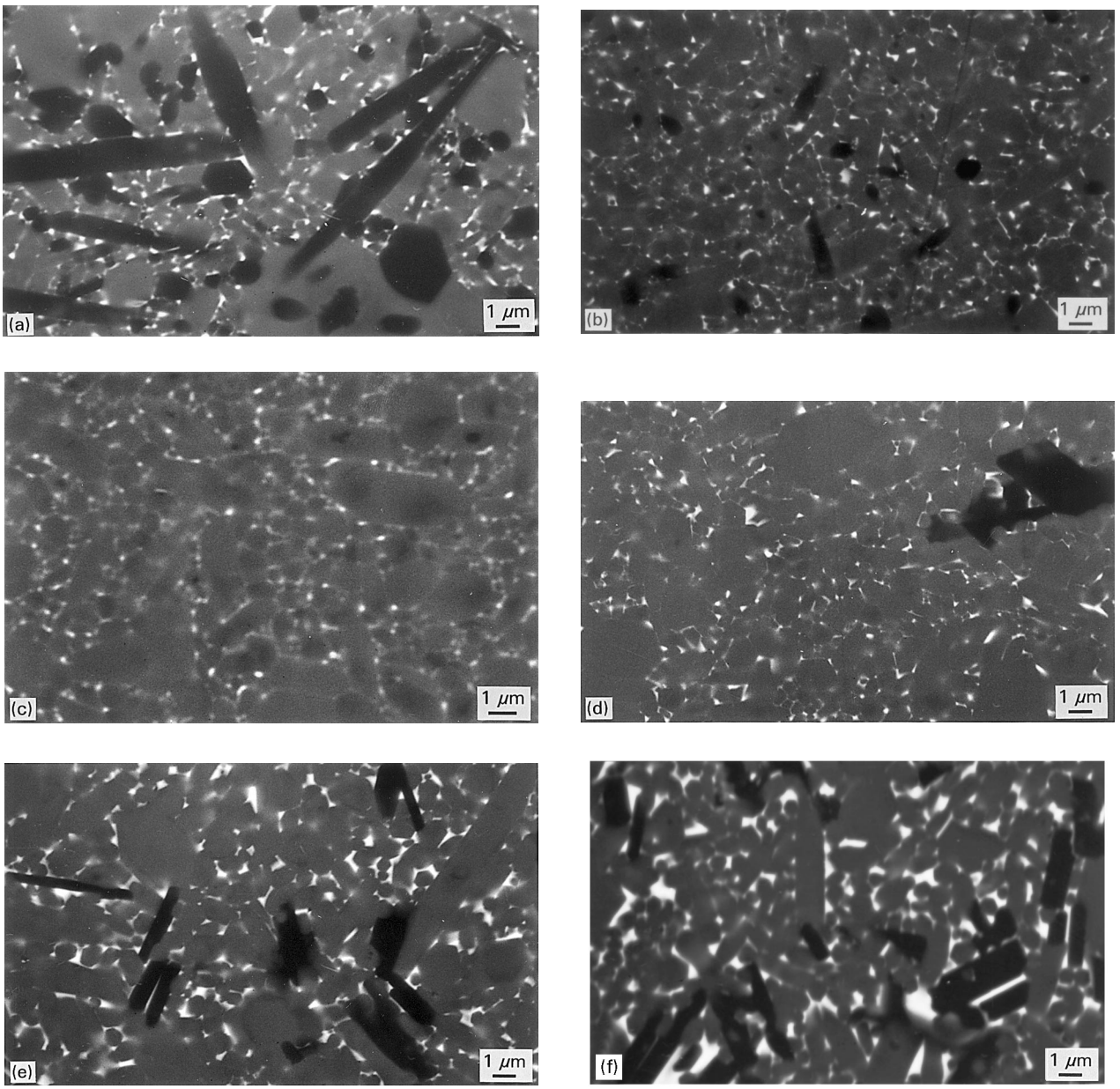

Figure 6 Back-scattered scanning electron micrographs of samples quenched from 1750 °C: (a) ADY025 ($x = 0.25$) , (b) ADY035, (c) ADY04, (d) ADY06, (e) ADY08 and (f) ADY10 ($x = 1.0$) , cf. text.

contrast. The presence of 21R sialon polytypoid crystals (in samples with high x values) is also easy to distinguish, because crystals of these phases are black and show elongated plate-like shapes.

The microstructure of the samples can be related to the three composition areas (I–III) described in Fig. 2a–c. The samples in the α–β phase range (area I) consisted of equi-axed α-grains with a wide size distribution ranging from 0.1–3 μm and elongated β-grains, see Fig. 6a and b. The aluminium content of the β-phase changes slightly when the overall x value increases from 0.2 to 0.25, shown by an increase of the z value from 0.37 to 0.42. It can be noted that the major amount of glassy phase is located at the multigrain junctions and the volume of glassy phase seems to decrease slightly with increasing x value, but thin films were always present between adjacent sialon grains.

The single-phase α-sialon samples (area II) consist predominantly of α grains surrounded by some residual intergranular glassy phase, and the content of glassy phase increases with increasing x value, cf. Fig. 6c and d. At higher x values, in area III, more complex microstructures occur. They contain α-sialon grains as the main phase, having elongated shapes to a greater extent than for samples with lower x values, see Fig. 6e and f. In area III, large amounts of glassy phase occur, and some elongated plate-like sialon polytypoid crystals (the 21R modification according to the XRD and EDS point analysis).

The formation of elongated α-sialon crystals in area III is probably promoted by the presence of large amounts of liquid at the sintering temperature. This is an interesting feature, as α-sialon has seldom been reported to have this crystal shape, contrary to β-sialon crystals. Recently, we have observed that the formation of elongated α-sialon crystals is not only promoted by large amounts of liquid but occurs more frequently for certain rare-earth dopants, and these findings will be reported elsewhere [19].

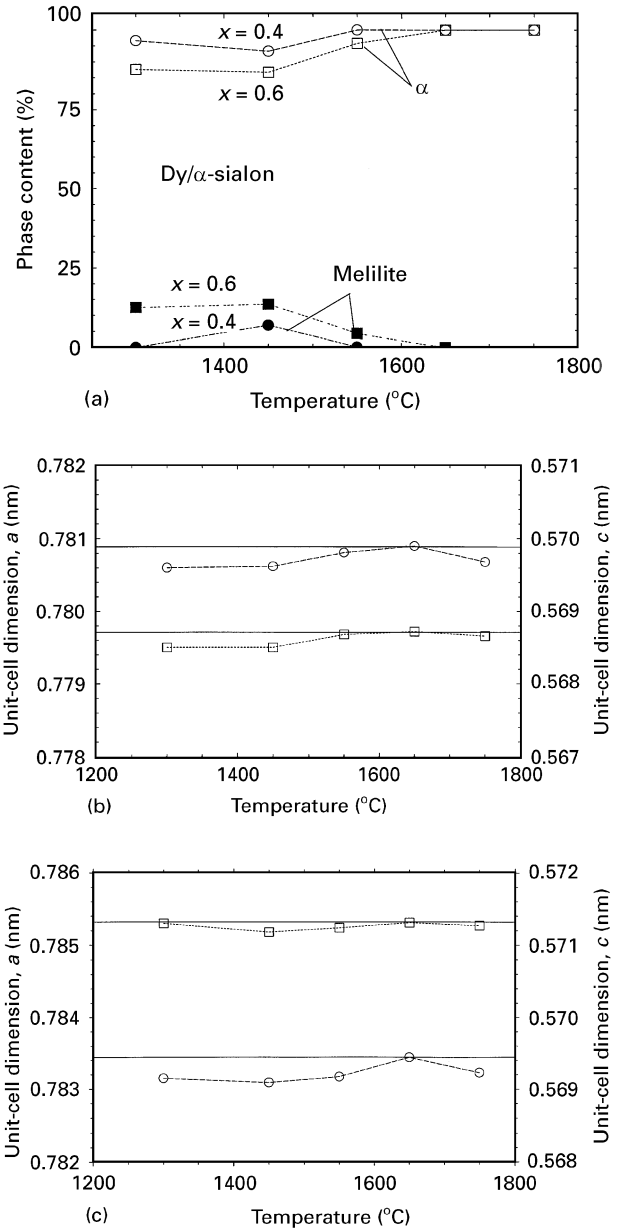

Figure 7 (a) Observed phase contents and (b, c) unit-cell dimensions of the samples (b) ADY04 and (c) ADY06 after heat treatment at different temperatures for 24 h. (○) a, (□) c.

3.2. Thermal and time stability of dysprosium-doped α-sialon

Two hot-pressed dysprosium-doped α-sialon samples with different overall x values, namely ADY04 ($x = 0.4$) and ADY06 ($x = 0.6$), were heat treated for 24 h at temperatures from 1300–1750 °C and then quenched. The phases present in these samples are shown in Fig. 7a. The corresponding unit cell parameters of α-sialon are shown in Fig. 7b and c. In ADY04 the M′ phase was observed only after heat treatment at 1450 °C, in a minor amount. It formed more easily and over a more extended temperature range in ADY06, i.e. at the higher overall x value, cf. Fig. 7a.

The formation of the M′-phase around 1450 °C seems to be accompanied by a slight decrease of the unit cell of the α-sialon. This indicates that the composition of the residual liquid phase at this temperature is slightly different from that of the formed M′-phase, $Dy_2Si_{2.3}Al_{0.7}O_{3.7}N_{3.3}$. The residual liquid and the α-sialon grains may thus have reacted in a limited scale to compensate for the composition difference between Dy-M′ and liquid

$$\text{liquid} + \alpha_1 \rightarrow Dy_2Si_{3-x}Al_xO_{3+x}N_{4-x} + \alpha_2 \qquad (4)$$

In the formation of Dy-M′, dysprosium and other elements are consumed from the residual liquid and in part from α-sialon. Similar reactions have been seen in the yttrium-, samarium-, neodymium- and ytterbium-doped α and α–β sialon systems [10–13]. In the case of ytterbium, however, a garnet type of phase, $Yb_3Al_5O_{12}$, is formed instead of melilite [13].

In order to investigate the time dependence of this reaction (Equation 4) the sample ADY04 was heat treated at 1450 °C for up to 30 days in a nitrogen atmosphere. The phases present and the corresponding unit cell dimensions of α-sialon after different heat-treatment times are given in Fig. 8a and b, respectively. These results show that the Dy-M′-phase is only formed during the first 24 h (accompanied by

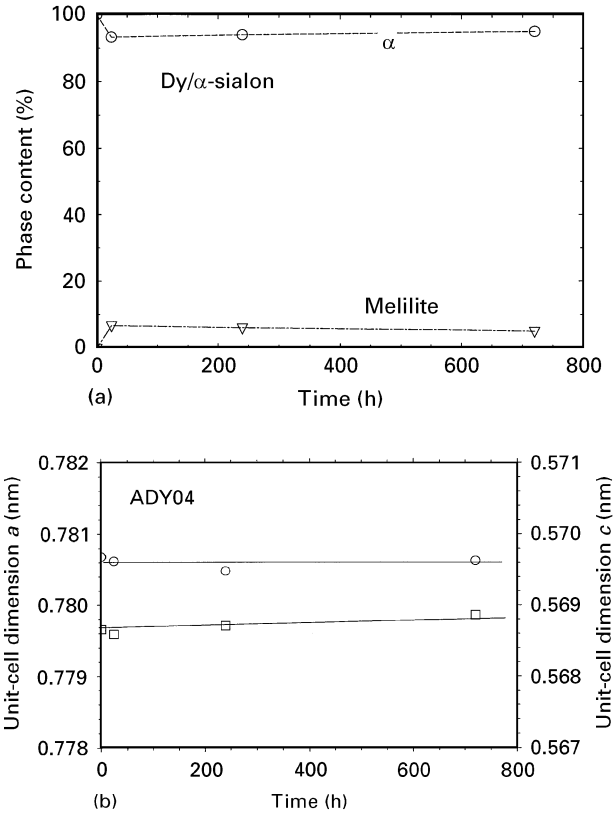

Figure 8 (a) The observed phases present in sample ADY04 and (b) the unit-cell dimensions of the α-sialon phase, after heat treatment at 1450 °C for 1–30 days. (○) *a*, (□) *c*.

a slight decrease of the α-sialon content), i.e. beyond the first day no further reactions take place. The behaviour is similar to that of ytterbium doped α-sialon, but different from that observed in corresponding neodymium- and samarium-doped α-sialon systems [11, 12]. In the latter cases, a rapid initial devitrification of the residual grain-boundary glassy phase, similar to the process indicated in Equation 4, does take place, but is followed by a further decomposition of α-sialon, whereby β-sialon and melilite are formed.

Scanning electron micrograph analyses reveal that the residual glassy grain-boundary phase already disappeared while the Dy-M′-phase was formed in sample ADY04 after heat treatment at 1450 °C for 24 h. Thus, the microstructure of the quenched sample consists of α-sialon grains surrounded by some residual glassy phase, which indicates that α-sialon forms in equilibrium with a liquid phase. After the heat treatment at 1450 °C for 1 day, Dy-M′-phase has been formed and the glassy phase consumed, and further heat treatment does not alter the microstructure.

The results obtained for the dysprosium system may be compared with our previous work on thermal stability of α-sialon in neodymium-, samarium- and ytterbium-doped systems [11–13]. Two different mechanisms seem to affect the stability of α-sialon: one where the composition of the α-sialon shifts and an M′- or garnet phase is formed, named the reaction-induced mechanism below; and the other implying that the α-sialon is decomposed directly into β-sialon and an appropriate intergranular phase. The reaction-induced mechanism operates in all rare-earth doped systems. The latter decomposition mechanism of the α-sialon is found only for the samarium- and neodymium-doped α-sialon phases. In these cases, α-sialon transforms to β-sialon plus one or more rare-earth-rich grain-boundary phase(s) at lower temperatures. The decomposition is strongly related to the kind and thermal stability of the rare-earth-rich grain-boundary phase(s) formed [11–13].

The M′-phase has been noticed to be effective in removing both rare-earth cations and nitrogen from α-sialon, and the competition for rare-earth ions between M′-phase and α-sialon seems to determine the stability of the α-sialon. In other words, the thermal stability of α-sialon can be seen as related to the stability of the M′-phase. It has been shown that large cations such as Nd^{3+} and Sm^{3+}, form stable M′-phases very easily; small cations such as Yb^{3+} never form the M′-phase, and medium-size cations such as Dy^{3+} and Y^{3+} are on the boundary of M′-phase formation [18]. Hence, in the case of neodymium and samarium the M′-phase seems to be more stable than the α-phase, whereas with ytterbium, dysprosium and yttrium, the α-phase is stable. It should be stressed, however, that if sialon ceramic with the latter elements contains considerable amounts of amorphous phase, the devitrification process and the compositional adjustments occurring during prolonged heat treatment (the system approaches equilibrium) might consume some α sialon, and this procedure can be misinterpreted as α-sialon decomposing directly.

3.3. Mechanical properties of sialon ceramics along the Si_3N_4–$Dy_2O_3 \cdot 9AlN$ join line

The Vickers hardness, $H_{v_{10}}$, and the indentation fracture toughness, K_{1c}, were measured for selected hot-pressed samples, and the results are given in Fig. 9. The general trend is that the mixed α–β sialon materials in area I (with an overall composition of $x < 0.35$) exhibited higher toughness but lower hardness than the α-sialons of area II. The hardness of mixed α–β sialon in area I increased with increasing α-sialon content, while the toughness decreased. The highest hardness values ($H_{v_{10}} = 21$–22 GPa) were obtained for materials in area II (with overall compositions of

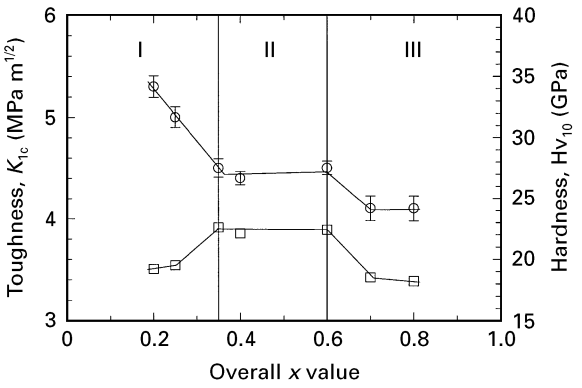

Figure 9 Measured (□) Vickers hardness, $H_{v_{10}}$, and (○) indentation toughness, K_{1c}, of samples along the Si_3N_4–$Dy_2O_3 \cdot 9AlN$ tie line, hot-pressed at 1800 °C for 2 h.

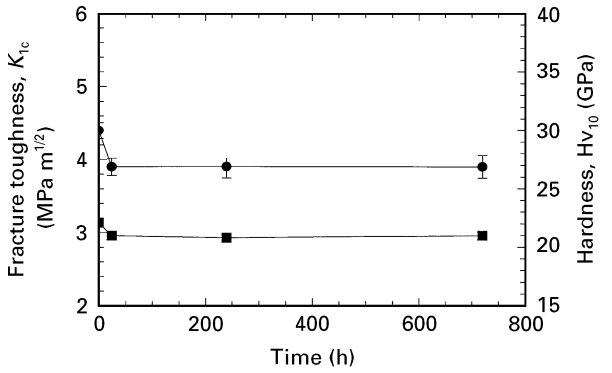

Figure 10 Measured (■) Vickers hardness, $H_{v_{10}}$, and (●) indentation toughness, K_{1c}, of sample ADY04 heat treated at 1450 °C, plotted as a function of heat-treatment time.

$0.35 \leqslant x \leqslant 0.6$). These results are in good agreement with previous findings concerning how $H_{v_{10}}$ and K_{1c} change when the α/β ratio changes [3, 20]. Besides α-sialon materials in area III (having overall x values larger than 0.6) contained more glassy phase, sialon polytypoids and the M′-phase. These materials were consequently found to be somewhat less hard. They were also more brittle, and the presence of elongated α-sialon crystals in these materials did not seem to contribute to an enhanced toughness.

The changes of Vickers hardness and indentation hardness as functions of the heat-treatment time at 1450 °C for the sample ADY04 ($x = 0.4$) are shown in Fig. 10. This illustrates that, although these properties decreased slightly after 24 h heat treatment, they are unaffected by prolonged heat-treatment time. The decrease of toughness might be due to the disappearance of the residual grain-boundary glassy phase, and the decrease of hardness may depend on the formation of the Dy-M′-phase, which is much softer ($H_{v_{10}} \approx 10$ GPa) than the α-sialon phase. The observation that the toughness and hardness are not degraded by further heat treatment is in agreement with the fact that no noticeable phase or microstructural changes occur during prolonged heat-treatment.

4. Conclusions

1. Dense dysprosium-doped sialon ceramics with overall compositions of $Dy_x\ Si_{12-4.5x}Al_{4.5x}O_{1.5x}N_{16-1.5x}$, with $0.2 \leqslant x \leqslant 1.0$ (along the Si_3N_4–$Dy_2O_3 \cdot 9AlN$ tie line) were prepared by hot-pressing at 1800 °C. The dysprosium-doped α-sialon phase is formed in the composition range $0.3 \leqslant x \leqslant 0.7$.

2. Materials of different compositions were post-heat-treated at temperatures in the range 1300–1750 °C for different times, and it was found that the Dy-α-sialon phase is stable over the whole temperature interval and during heat-treatment times up to 30 days at 1450 °C.

3. Initially, in the heat treatment at 1450 °C, the residual liquid grain-boundary phase reacted with minor amounts of the α-sialon phase during devitrification, yielding Dy-M′-phase and a glassy phase-free material. This might shift the α-sialon composition somewhat as indicated by Equation 4, but the reaction stops as soon as the residual glass is fully devitrified.

4. α-phase can coexist with a liquid phase at temperatures $\geqslant 1550$ °C and with Dy-M′-phase at $\leqslant 1450$ °C. Unlike in the corresponding neodymium- and samarium-doped α-sialon systems, dysprosium-doped α-sialon does not decompose on prolonged heating at $\leqslant 1450$ °C into β-sialon and some rare-earth-rich grain-boundary phase(s).

5. The Dy-M′-phase ($Dy_2Si_{3-x}Al_xO_{3+x}N_{4-x}$) coexisting with the α-phase was found to have the maximum possible aluminium substitution ($x = 0.7$) .

6. Dysprosium-doped α-sialon ceramics composed of α-sialon grains and a small amount of glassy grain-boundary phase exhibited very high hardness ($H_{v10} =$ 22 GPa) and a fracture toughness of 4.5 MPa m$^{1/2}$ and the hardness and toughness decreased only slightly after devitrification of the glassy phase.

7. At high x values of the α-sialon formula, elongated α-sialon grains were formed, but their presence did not affect the toughness significantly.

Acknowledgements

This study has been supported by the Swedish Research Council for Engineering Sciences. Zhijian Shen thanks the Swedish Institute for a scholarship during the period when the work was carried out.

References

1. K. H. JACK, in NATO ASI Series "Progress in Nurogen Ceramics", edited by F.L. Riley (Martinus Nijhoff, 1983) p. 45.
2. G. Z. CAO and R. METSELAAR, *Chem. Mater.* **3** (1991) 242.
3. T. EKSTRÖM and M. NYGREN, *J. Am. Ceram. Soc.* **75** (1992) 259.
4. T. EKSTRÖM, *Mater. Res. Soc. Symp. Proc.* **287** (1992) 121.
5. T. EKSTRÖM, *Mater. Forum* **17** (1993) 67.
6. S. HAMPSHIRE, H. K. PARK, D. P. THOMPSON and K H. JACK, *Nature* (*Lond.*) **274** (1978) 880.
7. Z. K. HUANG, T. Y. TIEN and T. S. YEN, *J. Am. Ceram. Soc.* **69** (1986) C-241.
8. W. Y. SUN, T. Y. TIEN and T. -S. YEN, *ibid.* **74** (1991) 2547.
9. H. MANDAL, D. P. THOMPSON and T. EKSTRÖM, *J. Eur. Ceram. Soc.* **12** (1993) 421.
10. T. EKSTRÖM and Z. J. SHEN, in "5th International Symposium on Ceramic Materials and Components for Engine", edited by D. S. Yan, X. R. Fu and S. X. Shi (World Scientific, Singapore, 1995) p. 206.
11. Z. J. SHEN, T. EKSTRÖM and M. NYGREN, *J. Eur. Ceram. Soc.*, **16** (1993) 43.
12. *Idem, J. Am Ceram Soc.*, **79** (3) (1996) 721.
13. *Idem, J. Hard Mater.*, **29** (1996) 893.
14. G. R. ANSTIS, P. CHANTIKUL, B. R. LAWN and D. P. MARSHALL, *J. Am. Ceram. Soc.* **64** (1981) 533.
15. K. -E. JOHANSSON, T. PALM and P. -E. WERNER, *J. Phys.* **E13** (1980) 1289.
16. P. -E. WERNER, *Arkiv Kemi* **31** (1969) 513.
17. T. EKSTRÖM, P. -O. KÄLL, M. NYGREN and P. -O. OLSSON, *J. Mater. Sci.* **24** (1989) 1853.
18. P. L. WANG, H. Y. TU, W. Y. SUN, D. S. YAN, M. NYGREN and T. EKSTRÖM, *J. Eur. Ceram. Soc.*, **15** (1995) 689.
19. L. -O. NORDBERG, Z. J. SHEN and T. EKSTRÖM, *J. Eur. ceram. Soc.*, **15** (1995) in press.
20. T. EKSTRÖM, *J. Hard Mater.* **4** (1993) 77.

Received 8 August
and accepted 21 December 1995